

Spaces of Curves, Dynamical Contours and Localization in Computer Vision*

Washington Mio [†] Anuj Srivastava [‡] Xiuwen Liu [§]

Abstract

Using techniques from computational differential geometry, we present a new approach to the algorithmic study of planar curves, with applications to shape and image analysis. The main idea is to construct spaces of curves satisfying constraints suited to specific problems and exploit the geometric structure of these spaces to quantify and analyze properties of contours and solve optimization and inference problems. Applications include: (i) new geometric algorithms for the estimation of contours and appearances of partially occluded objects in images; (ii) the development of a novel multi-resolution, algorithmic approach to statistical shape analysis using progressive localization in the frequency domain; (iii) algorithms for computing planar elasticae with enhanced performance and speed.

Contents

1	Introduction	2
1.1	Completion of Contours with Elasticae	3
1.2	Localization, Completion of Contours and Appearances	4
1.3	Frequency Localization and Shape Analysis	5
2	Representation of Planar Curves	5
2.1	A Manifold of Constrained Curves	6
2.2	The Normal Bundle of \mathcal{A}	7
2.3	Projection onto \mathcal{A}	8
3	Scale-Invariant Planar Elasticae	9
3.1	The Elastic Energy Flow	9
3.2	Algorithms and Experimental Results	10
4	Localization of Curvature and Angle Functions	11
4.1	V -Local Curves	11
4.2	V -Local Elasticae	14

*Submitted to a special issue of the International Journal of Computer Vision.

[†]Department of Mathematics, Florida State University, Tallahassee, FL 32306

[‡]Department of Statistics, Florida State University, Tallahassee, FL 32306

[§]Department of Computer Science, Florida State University, Tallahassee, FL 32306

5	Discovery of Contours and Appearances	15
5.1	A Manifold of Localized Closed Curves	15
5.2	Bayesian Estimation of Contours	16
5.3	Algorithms and Experimental Results	17
6	Spaces of Localized Shapes	18
6.1	Localization of Pre-Shapes	20
6.2	Geodesics in the Shape Space \mathcal{S}_n	21
7	Acknowledgments	22

1 Introduction

The detection, recognition and classification of objects in images are central problems in computer vision, whose study is motivated by numerous applications such as medical image analysis and recognition of objects using X-ray or infrared images. The past decade has seen significant advances in modeling appearances of objects in images, but the methods have been applied to recognition and classification only with limited success. This is due, in part, to difficulties related to partial occlusions of objects that are frequently present in images and to the high variability of observed pixel values caused by factors such as illumination, pose, scale and noise. Thus, it is important to take into account additional global features of objects such as shapes of contours and their variations in order to develop high performance image analysis algorithms. This motivates a geometrical approach to the representation and statistical analysis of planar curves for applications in computer vision.

In this paper, using techniques of differential geometry, we present a novel framework for the algorithmic study of planar curves and apply the methodology developed to obtain new algorithms for the completion of partial occlusions of contours in images and for multi-resolution shape analysis. Curves are treated as *continua* and discrete formulations are used only at the implementation level. Thus, representations of curves often involve infinitely many degrees of freedom, which lead us to the study of the geometry of both finite and infinite-dimensional manifolds. In our approach, a fundamental element is a *space of constrained curves*, referred to as SCC henceforth. As an example, if we are interested in analyzing closed curves that outline objects in images, the *closure condition* provides a constraint. Many other constraints on curves that arise naturally in image understanding are investigated in this paper. We emphasize that although some spaces of curves considered are finite dimensional, most SCCs are nonlinear, infinite-dimensional manifolds, whose elements are the individual curves of interest.

A typical SCC is a *smooth manifold* equipped with a *Riemannian structure*; that is, a manifold with an inner product on each tangent space that varies smoothly along the space. Once such structure is available, geometric quantities such as the length of a curve, geodesic distances and curvatures can be defined and calculated in an intrinsic manner. For example, if M is a Riemannian manifold and $\alpha: I \rightarrow M$ is a curve on M , the usual expression $\int_I \sqrt{\langle \alpha'(t), \alpha'(t) \rangle} dt$ can be used to define the length of α . We exploit the geometry of SCCs for an algorithmic study of geodesic and gradient flows on these Riemannian manifolds and apply the techniques developed to the solution of optimization and statistical inference problems associated with a variety of cost functions and probability models on these spaces. Kendall's shape spaces [12], constructed from landmark

representations of contours, can be viewed as finite-dimensional precursors to SCCs. Of particular historical significance is the fact that Kendall’s spaces motivated the study of statistics in general finite-dimensional Riemannian manifolds [16, 27, 6].

Active contours, which are essential components of many image analysis algorithms, have been the subject of numerous studies since the introduction of “snakes” in [11]. In this approach, dynamical contours are typically driven by data and smoothness energies, and their evolution is governed by partial differential equations (PDEs). Level-set methods form the basis of another widely used PDE-based approach to the algorithmic analysis of contours (see e.g. [25, 2]). *Given the past success of PDE-based approaches to dynamical contours, why introduce new methodology?* The study of the geometric structure of SCCs provides new insights and solutions to problems involving planar contours and problems in quantitative shape and image analysis, as demonstrated in many applications investigated in this paper (see also [14, 9, 20]). An important characteristic that distinguishes the present treatment of curves from those employed in previous algorithmic studies of “geometry-driven flows” [23] is that there is a well-defined, structured space of curves on which optimization and inference problems can be formulated and statistical models developed. In our approach, both the geometry of curves and the geometry of spaces of curves are utilized. The dynamics of active contours is modeled on vector fields on SCCs, which are constructed and integrated numerically using geometrical properties of SCCs. This reduction of curve evolution to the integration of vector fields leads to algorithms with improved computational efficiency, as exemplified by our algorithm for computing planar *elasticae*, discussed in more detail below. As further evidence of the benefits of this approach to the study of planar curves, the geometry of SCCs was used in [14, 20] to construct probability models, define means and covariance operators in infinite-dimensional shape spaces; only rarely have these quantities received a formal treatment in previous studies of statistics in non-linear, infinite-dimensional manifolds. Statistical studies of planar curves using PDE methods have been undertaken in [3, 18, 4], but developments in this direction are still incipient.

We should also point out the main limitations of the proposed approach to the analysis of edges and contours in images. One drawback is that curve evolution cannot handle changes in topology, which is one of the key features of level-set methods; a SCC is purposely designed to not allow components of a curve to branch or merge. Secondly, this formulation does not extend easily to the analysis of surfaces in 3D space or hypersurfaces in n -dimensional Euclidean space. Despite these limitations, the proposed methodology leads to powerful new geometric algorithms for the analysis of planar curves as demonstrated in many applications.

We now give a brief description of several SCCs that are investigated in this paper along with problems in shape and image analysis that motivate their study.

1.1 Completion of Contours with Elasticae

The estimation of contours of partially occluded objects in images is, in general, a difficult problem. The *elastica model* for the completion of visible edges was introduced in computer vision in [8], but the study of the elastic energy of curves dates back to Euler [7]. This model yields particularly good results when occlusions are fairly small or not very rich in geometric features, as exemplified by the oranges in Fig. 1(a). The estimation of illusory contours in images such as the well-known Kanizsa’s triangle [10], shown in Fig. 1(b), involves problems of similar nature [21, 30]. However, *elasticae* do not satisfactorily resolve occlusions such as those shown in Figs. 1(c) and 1(d). Mumford [21] gave an stochastic interpretation to *elasticae* as the most likely curves according to a probability model based on length and (bending) elastic energy. In [29, 1], it was argued that scale-invariant models are



Figure 1: Examples of partially occluded and illusory contours in images. Hidden boundaries in (c) and (d) have more geometric features than in (a) making the estimation more difficult.

more natural in vision problems and the notion of *scale-invariant elasticae* was introduced. Further studies of elasticae and associated stochastic completion fields were carried out by Williams and Jacobs [30, 31], but calculations were computationally very intensive. Algorithmically efficient approximations were investigated in [26] by Sharon et al. under the simplifying assumption that elasticae could be described as graphs of functions. More recently, Mio et al. [19] developed an efficient geometric algorithm to compute general elasticae in arbitrary Euclidean spaces. In [13], Kimia et al. investigated completions of contours with Euler spirals.

As an application of SCCs, in this paper, we develop a higher performance algorithm for the calculation of elasticae in the plane \mathbb{R}^2 . Not only we achieve improved computational efficiency and simplify the algorithm of [19] by restricting the analysis to the 2D case, but the algorithm can be modified to compute a new type of elasticae that we introduce in this paper, namely, *local elasticae* with curvature functions localized in the frequency domain, as discussed below. We will focus the discussion on scale-invariant elasticae, but the algorithm can be easily modified for calculations of other types of elasticae, as in [19]. Here, the relevant SCC consists of all curves with prescribed first-order boundary conditions; that is, curves with prescribed position and direction at the initial and terminal points. The Riemannian structure on this infinite-dimensional manifold and precise assumptions on the regularity of curves will be discussed later. The goal is to find the curve C that minimizes the *scale-invariant elastic energy* defined as

$$(1.1) \quad E(C) = \frac{L}{2} \int_C \kappa_C^2(s) ds,$$

where L is the length of C and κ_C the curvature of C . The minimization problem is solved with a gradient search on the SCC.

1.2 Localization, Completion of Contours and Appearances

The curve completions with elasticae discussed in Sec. 1.1 are based solely on the minimization of the scale-invariant elastic energy and first-order boundary conditions. As such, they disregard a substantial amount of geometric data available and it seems natural to seek completions that use more information from the visible parts of contours, especially in situations where some geometric pattern is observed. We propose to constrain the search to curves whose curvature functions are localized in the frequency domain, with just enough harmonics to be able to reproduce the main visible patterns. The underlying idea is that using localization of curvature functions to their lower harmonics, the main observed geometric features will propagate to the parts to be estimated without a high elastic energy expenditure. We investigate two types of completions using curves with curvature functions localized in the frequency domain. First, we consider a new type of

completion with *local elastica*; that is, with a curve of minimal elastic energy satisfying prescribed first-order boundary conditions. We then study finer Bayesian estimations of the full contour using available data and an elastic energy prior. Whereas frequency localization of curvature may be difficult to achieve in a level-set or “snakes” approach, our methods allow us to construct SCCs of curves with localized curvature functions where the above inference problems are formulated and solved. Completions with curves whose curvatures are localized in the frequency domain yield better estimations of contours exhibiting periodic patterns such as those in Figs. 1(c) and 1(d).

Completion of contours of imaged objects will be complemented with texture analysis-synthesis techniques developed in [32, 28, 17] to extend observed patterns of pixel values to the newly discovered regions. This fusion of shape and texture analysis techniques provides new methodology for estimations of the full appearance of partially occluded objects. Many existing in-painting algorithms are developed in a level-set framework and rely on PDE methods; the reader may consult the survey article [2] for recent results in this direction. Our approach differs significantly from the viewpoint of techniques employed as it involves a combination of methods of differential geometry of infinite-dimensional Riemannian manifolds for the study of contours and decompositions of images into their spectral components using bandpass filters for analysis and synthesis of textures. The methods developed in this paper allow us to resolve fairly large occlusions with non-trivial geometry and texture patterns, as demonstrated in several experiments.

1.3 Frequency Localization and Shape Analysis

In [14], using geometric representations of closed contours by angle or curvature functions, Klassen et al. introduced and developed a new statistical theory of continuous, planar shapes. The main tool employed is a geometric algorithm for the calculation of geodesics in shape space. Geodesics and geodesic distances are used to quantify shape dissimilarities, interpolate and extrapolate shapes, define mean shapes, covariance operators and develop statistical models in shape space. The techniques developed in [14] were applied to shape clustering, learning and hypothesis testing in [9] and to recognition and detection of shapes in images with noise and partial occlusions in [20]. In practice, it is often the case that one wants to classify or identify imaged objects as belonging to certain known classes of objects adopting shape as a criterion. In order to optimize the balance of performance and efficiency in shape analysis algorithms, we develop a multi-resolution analogue of the representation and analysis of shapes of [14], using localization of angle functions in the frequency domain. The goal is to be able to tune shape representations to specific problems using just enough harmonics to capture sufficient geometric information about shapes of interest. To illustrate the idea, the leftmost panel in each row of Fig. 2 shows a shape extracted from a natural image. The other panels show representations of the shape, at various different resolutions, obtained using a frequency localization procedure described in Sec. 6. Dotted lines represent the original shapes and localized shapes are drawn as solid lines.

An algorithm to compute geodesic paths between shapes localized in the frequency domain will be described in Sec. 6, so that the algorithmic methods of statistical shape analysis of [14, 9, 20] can be adapted to shape representations at arbitrary resolutions.

2 Representation of Planar Curves

We study planar curves presented in parametric form and traversed with constant speed. More precisely, we consider curves $\alpha: I \rightarrow \mathbb{R}^2$ parameterized over the unit interval $I = [0, 1]$ with $\|\alpha'(s)\|$

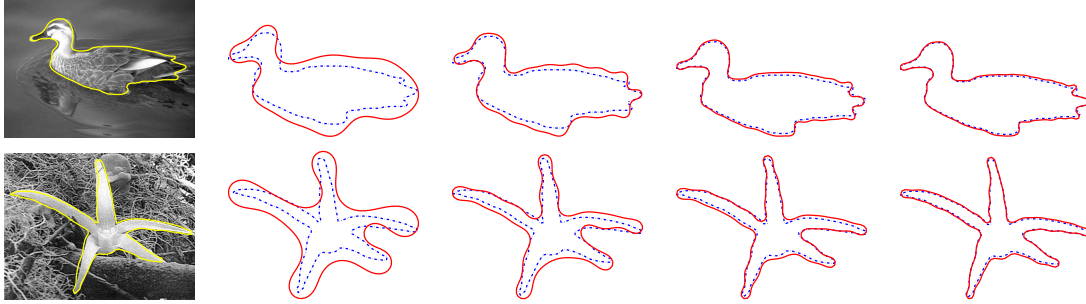


Figure 2: Shapes extracted from natural images are represented at various different resolutions.

constant. Thus, if the length of α is L , $\|\alpha'(s)\| = L$, for every $s \in I$. A continuous function $\theta: I \rightarrow \mathbb{R}$ is said to be an *angle function* for α if $\alpha'(s) = Le^{j\theta(s)}$, for every s , where $j = \sqrt{-1}$. Here, we are identifying \mathbb{R}^2 with the complex plane \mathbb{C} in the usual manner. Notice that angle functions are only defined up to the addition of integer multiples of 2π . Moreover, they are invariant to uniform scalings and translations of the curve; the effect of a rotation is to add a constant to θ . The *rotation index* of α , which measures the total number of turns made by the tangent vector $\alpha'(s)$ as the curve α is traversed, is defined as

$$(2.1) \quad \iota(\alpha) = \frac{1}{2\pi} (\theta(1) - \theta(0))$$

and is independent of the angle function chosen. The rotation index of a closed curve α with $\alpha'(0) = \alpha'(1)$ is an integer, with the sign depending on the orientation of the curve. If, in addition, α is a *simple* curve (i.e., with no self-intersections other than the end points) the rotation index is known to be ± 1 (see e.g. [5]).

Associated with α , there is a normalized unit-speed curve $\beta: I \rightarrow \mathbb{R}^2$ obtained by scaling α to have unit length; i.e., $\beta(s) = \alpha(s)/L$. If $\alpha'(s) = Le^{j\theta(s)}$, then $\beta'(s) = e^{j\theta(s)}$. Thus, any angle function for α is also an angle function for β and $\kappa(s) = \theta'(s)$ is the curvature function of β . Since curvature scales inversely, the curvature of α at s is $\kappa(s)/L$.

In applications involving the elastic energy, we must restrict allowable curves to those having square integrable curvature functions. Thus, we only consider angle functions $\theta: I \rightarrow \mathbb{R}$ that can be expressed as integrals of square integrable functions. In more technical terms, we assume that angle functions are *absolutely continuous* (see e.g. [24] for a precise definition) with square integrable first derivatives. The space of all such functions equipped with the inner product

$$(2.2) \quad \langle f, g \rangle_1 = f(0)g(0) + \int_0^1 f'(s)g'(s) ds,$$

is denoted \mathbb{H}^1 . This inner product – introduced by Palais in [22] – is a variant of the Sobolev inner product $\int_0^1 f(s)g(s) ds + \int_0^1 f'(s)g'(s) ds$. The usual \mathbb{L}^2 inner product $\int_0^1 f(s)g(s) ds$ is not appropriate in this context, since the elastic energy involves the \mathbb{L}^2 -norm of $\kappa(s) = \theta'(s)$.

2.1 A Manifold of Constrained Curves

We begin the discussion of SCCs by considering the space of all planar curves with square integrable curvature function, fixed rotation index, and given first-order boundary conditions. Thus, we

prescribe the endpoints $p_0, p_1 \in \mathbb{R}^2$ and angles $\theta_0, \theta_1 \in \mathbb{R}$ that determine the tangent directions at the endpoints. Our goal is to construct a SCC, denoted \mathcal{A} , consisting of all curves α of rotation index $(\theta_1 - \theta_0)/2\pi$ satisfying $\alpha(i) = p_i$ and $\alpha'(i)/\|\alpha'(i)\| = e^{j\theta_i}$, for $i = 0, 1$.

Using a logarithmic scale for the length, write $L = e^\ell$. If θ is an angle function for α , the velocity vector can be written as $\alpha'(s) = e^\ell e^{j\theta(s)}$. Thus, curves of length L satisfying $\alpha(0) = p_0$ can be expressed in the form

$$(2.3) \quad \alpha(s) = p_0 + e^\ell \int_0^s e^{j\theta(\sigma)} d\sigma.$$

Let $d = (d_1, d_2) = p_1 - p_0$ be the desired total displacement of α . Then, the condition $\alpha(1) = p_1$ can be written as $e^\ell \int_0^1 e^{j\theta(s)} ds = d_1 + jd_2$, or equivalently, as the following conditions on the total horizontal and vertical displacements of α :

$$(2.4) \quad e^\ell \int_0^1 \cos \theta(s) ds = d_1 \quad \text{and} \quad e^\ell \int_0^1 \sin \theta(s) ds = d_2.$$

Hence, there is a one-to-one correspondence between elements of \mathcal{A} and pairs $(\ell, \theta) \in \mathbb{R} \times \mathbb{H}^1$ satisfying $\theta(0) = \theta_0$, $\theta(1) = \theta_1$ and (2.4). These four constraints define a codimension-4 submanifold of $\mathbb{R} \times \mathbb{H}^1$; i.e., a submanifold of $\mathbb{R} \times \mathbb{H}^1$ whose normal space at each point is four dimensional. We are assuming that the ambient space $\mathbb{R} \times \mathbb{H}^1$ is equipped with the inner product

$$(2.5) \quad \langle (v, f), (w, g) \rangle = v \cdot w + \langle f, g \rangle_1,$$

where $(v, f), (w, g) \in \mathbb{R} \times \mathbb{H}^1$. See Fig. 3(a) for a schematic illustration of the local structure of a SCC.

Before proceeding with the calculations, we describe the space \mathcal{A} as a level set, as this will shed some light on its geometric structure. Define a function $F: \mathbb{R} \times \mathbb{H}^1 \rightarrow \mathbb{R}^4$ by:

$$(2.6) \quad \begin{aligned} F^1(\ell, \theta) &= e^\ell \int_0^1 \cos \theta(s) ds; & F^2(\ell, \theta) &= e^\ell \int_0^1 \sin \theta(s) ds; \\ F^3(\ell, \theta) &= \theta(0); & F^4(\ell, \theta) &= \theta(1). \end{aligned}$$

Then, \mathcal{A} is the level set $F^{-1}(d_1, d_2, \theta_0, \theta_1)$. Note that F^3 and F^4 are linear functionals on $\mathbb{R} \times \mathbb{H}^1$ and can be expressed in terms of the inner product $\langle \cdot, \cdot \rangle$ as $F^3(\ell, \theta) = \langle (\ell, \theta), (0, 1) \rangle$ and $F^4(\ell, \theta) = \langle (\ell, \theta), (0, 1 + s) \rangle$, where 1 and s denote the constant function 1 and the function $s \mapsto s$, respectively.

2.2 The Normal Bundle of \mathcal{A}

We will exhibit an explicit basis for the normal space to the level sets of F at any regular point $(\ell, \theta) \in \mathbb{R} \times \mathbb{H}^1$; that is, at any point where the derivative $dF: T_{(\ell, \theta)}\mathcal{A} \rightarrow \mathbb{R}^4$ is an onto mapping. Here, $T_{(\ell, \theta)}\mathcal{A}$ is the tangent space of \mathcal{A} at the point (ℓ, θ) . The derivative of F at (ℓ, θ) in the direction of the vector $(v, f) \in \mathbb{R} \times \mathbb{H}^1$ is given by:

$$(2.7) \quad \begin{aligned} dF^1(v, f) &= \left\langle (v, f), \left(F^1(\ell, \theta), e^\ell h_1 \right) \right\rangle; & dF^2(v, f) &= \left\langle (v, f), \left(F^2(\ell, \theta), e^\ell h_2 \right) \right\rangle; \\ dF^3(v, f) &= \langle (v, f), (0, 1) \rangle; & dF^4(v, f) &= \langle (v, f), (0, 1 + s) \rangle, \end{aligned}$$

where $h_1, h_2: I \rightarrow \mathbb{R}$ are characterized by $h_1''(s) = \sin \theta(s)$, $h_1(0) = h_1'(0) = 0$ and $h_2''(s) = -\cos \theta(s)$, $h_2(0) = h_2'(0) = 0$. This means that the gradient of F^i , $1 \leq i \leq 4$, is:

$$(2.8) \quad \begin{aligned} \nabla F^1(\ell, \theta) &= \left(F^1(\ell, \theta), e^\ell h_1 \right); & \nabla F^2(\ell, \theta) &= \left(F^2(\ell, \theta), e^\ell h_2 \right); \\ \nabla F^3(\ell, \theta) &= (0, 1); & \nabla F^4(\ell, \theta) &= (0, 1 + s). \end{aligned}$$

Hence, a vector (v, f) is tangent to the level set of F at (ℓ, θ) if and only if it is orthogonal to the subspace of $\mathbb{R} \times \mathbb{H}^1$ spanned by $\{\nabla F^i(\ell, \theta), 1 \leq i \leq 4\}$. We thus have constructed a basis of the normal space to the level set of F at any regular point (ℓ, θ) . An orthonormal basis can be obtained using the Gram-Schmidt process.

In applications, the calculation of normal structures will be useful in the computation of the gradient of energy functionals on \mathcal{A} . We usually proceed in two steps: first, calculate the gradient of the energy as a functional on $\mathbb{R} \times \mathbb{H}^1$, which is often an easier task. Then, subtract the normal component to \mathcal{A} to obtain the gradient as a functional on \mathcal{A} .

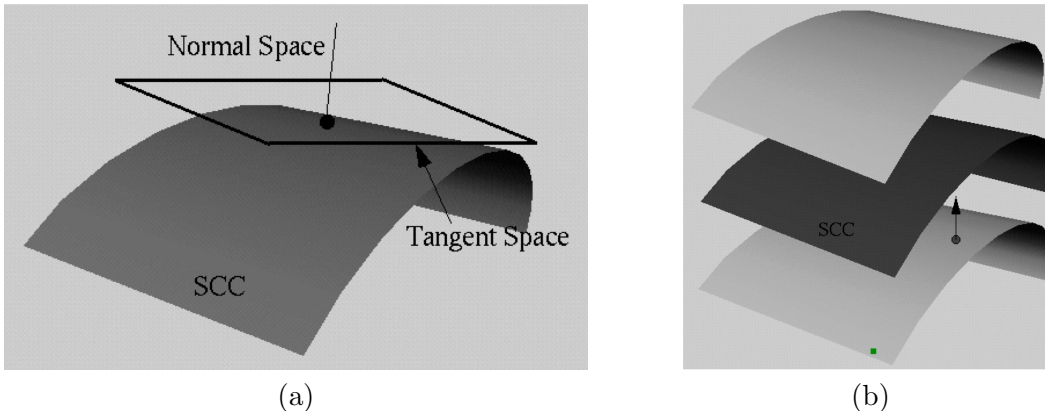


Figure 3: (a) The local structure of a SCC. (b) A SCC is a level set; points are projected onto the SCC by displacing them orthogonally to other level sets until the SCC is reached.

2.3 Projection onto \mathcal{A}

In numerical simulations of the flow associated with vector fields on \mathcal{A} , we use a variant of Euler's method, as follows. Infinitesimally, first flow in the ambient linear space $\mathbb{R} \times \mathbb{H}^1$ in the direction of the vector field. The new point typically falls off of \mathcal{A} due to its nonlinearity, so we devise a mechanism to project the point back onto \mathcal{A} to iterate the procedure – see Fig. 3(b). Higher-order integration methods can be modified similarly.

Let $(\ell, \theta) \in \mathbb{R} \times \mathbb{H}^1$. The residual vector $r(\ell, \theta) = (d_1, d_2, \theta_0, \theta_1) - F(\ell, \theta) \in \mathbb{R}^4$ is zero precisely at points $(\ell, \theta) \in \mathcal{A}$. Thus, $\varepsilon(\ell, \theta) = \|r(\ell, \theta)\|^2$ gives a measurement of how far off (ℓ, θ) is from \mathcal{A} and ε achieves its minimum value 0 at points in \mathcal{A} . We project (ℓ, θ) onto \mathcal{A} by following the negative gradient flow on $\mathbb{R} \times \mathbb{H}^1$ associated with the functional ε . The gradient of ε is given by

$$(2.9) \quad \nabla \varepsilon(\ell, \theta) = - \sum_{i=1}^4 r_i(\ell, \theta) \nabla F^i(\ell, \theta),$$

with $r = (r_1, r_2, r_3, r_4)$ and ∇F^i as in (2.8). Hence, the projection of a point $(\ell_*, \theta_*) \in \mathbb{R} \times \mathbb{H}^1$ onto \mathcal{A} is obtained by asymptotically following the solution of the initial value problem

$$(2.10) \quad (\dot{\ell}, \dot{\theta}) = \sum_{i=1}^4 r_i(\ell, \theta) \nabla F^i(\ell, \theta), \quad \ell(0) = \ell_*, \quad \theta(0) = \theta_*.$$

Alternatively, one can use a version of Newton's method to search for the zeros of r , in order to project points $(\ell, \theta) \in \mathbb{R} \times \mathbb{H}^1$ onto \mathcal{A} , as in [14, 19].

Algorithm 1 [Projection onto \mathcal{A}]: Given a pair $(\ell, \theta) \in \mathbb{R} \times \mathbb{H}^1$, we present an algorithm to project it onto \mathcal{A} , for a given d_1, d_2, θ_0 and θ_1 . Choose $\epsilon, \delta > 0$ small.

1. Compute $F(\ell, \theta)$ using Eqn. 2.6 and the residual vector $r(\ell, \theta) = (d_1, d_2, \theta_0, \theta_1) - F(\ell, \theta)$. If $\|r(\ell, \theta)\| < \epsilon$, then stop. Else, continue.
2. Compute $\nabla F^i(\ell, \theta)$, for $i = 1, \dots, 4$, according to Eqn. 2.8.
3. Compute $(\dot{\ell}, \dot{\theta})$ according to Eqn. 2.10.
4. Update $(\ell, \theta) = (\ell, \theta) + \delta(\dot{\ell}, \dot{\theta})$. Return to Step 1.

Shown in Fig. 4 are three examples of projections onto \mathcal{A} of curves represented by pairs (ℓ, θ) .

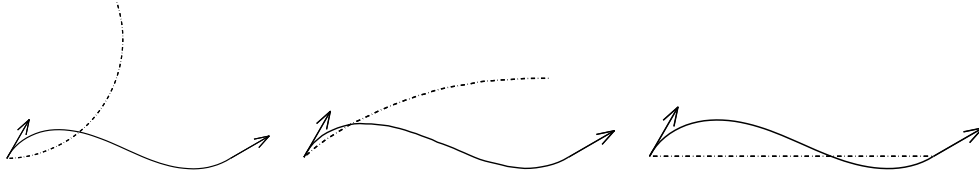


Figure 4: Examples of curves (dashed lines) and their projections (solid lines) onto \mathcal{A} using Algorithm 1.

3 Scale-Invariant Planar Elasticae

Let $(\ell, \theta) \in \mathcal{A}$ represent a curve $\alpha: I \rightarrow \mathbb{R}^2$ of length $L = e^\ell$ and let $\kappa(s) = \theta'(s)$. The (bending) *elastic energy* of α is the integral of the square of the curvature function κ/L with respect to the arc-length parameter. Since the arc-length element is $L ds$, the elastic energy of α can be expressed as $E(\ell, \theta) = \frac{1}{2L} \int_0^1 \kappa^2(s) ds$. The *scale-invariant elastic energy* of α [1], which is the product of E and the length L , is given by

$$(3.1) \quad E_{si}(\ell, \theta) = \frac{1}{2} \int_0^1 \kappa^2(s) ds.$$

3.1 The Elastic Energy Flow

The main goal of this section is to develop an efficient algorithm to calculate curves of least scale-invariant elastic energy with prescribed rotation index and first-order boundary conditions; these curves are known as *scale-invariant elasticae*. Equivalently, we wish to minimize the functional E_{si} on the manifold \mathcal{A} . From (3.1), the differential of E_{si} (as a functional on $\mathbb{R} \times \mathbb{H}^1$) at the point (ℓ, θ) evaluated in the direction (v, f) is

$$(3.2) \quad dE_{si}(v, f) = \int_0^1 f'(s)\theta'(s) ds = \langle (v, f), (0, \theta - \theta_0) \rangle.$$

Thus, $\nabla_{\mathbb{R} \times \mathbb{H}^1} E_{si}(\ell, \theta) = (0, \theta - \theta_0)$. Using the calculation of normal spaces to \mathcal{A} carried out in Sec. 2.2, we project this vector orthogonally onto the tangent space $T_{(\ell, \theta)}\mathcal{A}$ to obtain $\nabla_{\mathcal{A}} E_{si}(\ell, \theta)$. Flow lines of the negative gradient vector field on \mathcal{A} associated with E_{si} approach scale-invariant elasticae, asymptotically. For an analytical study of this flow in the case of closed curves, the reader may consult [15].

3.2 Algorithms and Experimental Results

Algorithm 2 [Finding Elasticae]: Given boundary conditions $(d_1, d_2; \theta_0, \theta_1)$, find the corresponding scale-invariant elastica. Initialize (ℓ, θ) with a straight line segment between the end points.

1. Project (ℓ, θ) onto \mathcal{A} using Algorithm 1.
2. Compute $e_i \equiv \nabla F^i(\ell, \theta)$, for $i = 1, \dots, 4$, according to Eqn. 2.8. Obtain an orthonormal basis using the Gram-Schmidt process:

```

for  $i = 1 : 4$ 
  for  $j = 1 : i - 1$ 
     $e_i = e_i - \langle e_i, e_j \rangle e_j$ ;
  end
   $e_i = e_i / \sqrt{\langle e_i, e_i \rangle}$ ;
end

```

3. Compute the gradient vector $(0, \theta - \theta_0)$ and project it onto the tangent space using:

$$(d\ell, d\theta) \equiv (0, \theta - \theta_0) - \sum_{i=1}^4 \langle (0, \theta - \theta_0), e_i \rangle e_i .$$

If $\|(d\ell, d\theta)\| < \epsilon$, stop. Else, continue.

4. For a step size $\delta > 0$, perform the update: $(\ell, \theta) = (\ell, \theta) + \delta(d\ell, d\theta)$. Return to Step 1.

Fig. 5 shows an application of this geometric algorithm to the calculation of a scale-invariant elastica for a given set of boundary conditions. Several stages of the curve evolution are shown, as well as a plot of the evolution of the scale-invariant elastic energy. Fig. 6 shows several other

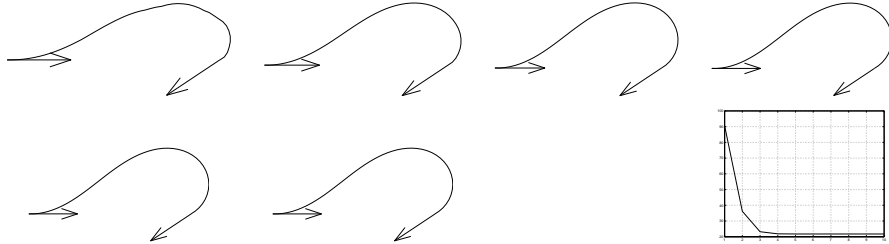


Figure 5: Evolution of a curve under the elastic energy flow. The last panel shows the corresponding evolution of energy.

examples of planar, scale-invariant elasticae. Elasticae with different rotation indexes are shown in Fig. 7.

Examples of partial occlusion of contours in natural images resolved with scale-invariant elasticae are shown in Fig. 8. The curves drawn as solid lines are elasticae computed with the algorithm developed in this section. For comparison purposes, dashed lines show hand-drawn contours.

Completion of contours of imaged objects with elasticae can be complemented with texture analysis-synthesis techniques developed in [32, 28, 17] to extend observed patterns of pixel values

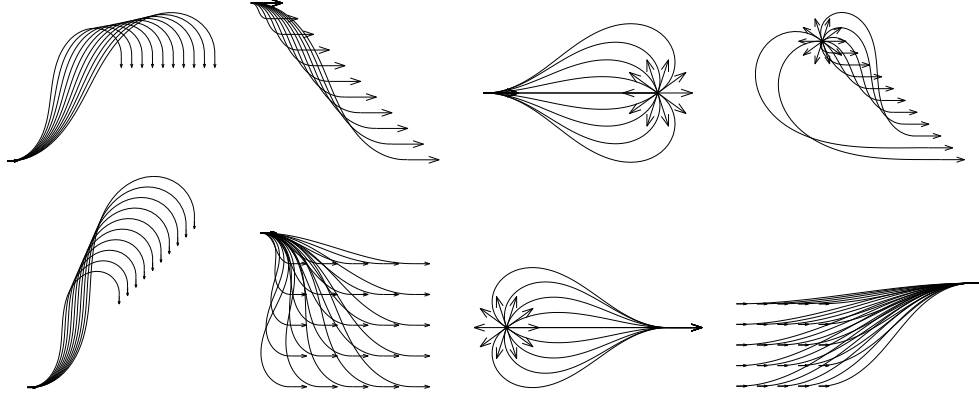


Figure 6: Examples of scale-invariant planar elasticae.

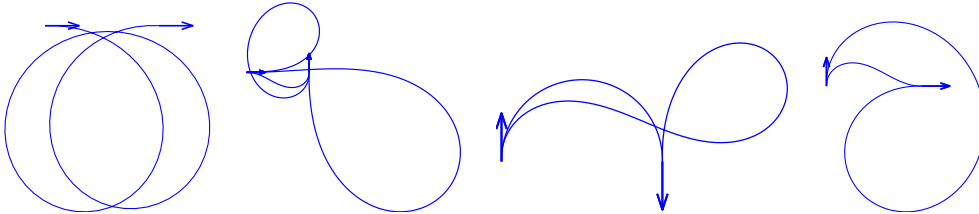


Figure 7: Examples of scale-invariant elasticae of different rotation indexes.

to the newly discovered regions. This fusion of shape and texture analysis techniques provides new methodology for estimations of the full appearance of partially occluded objects. Two examples of contour-appearance completions are shown in Fig. 9.

4 Localization of Curvature and Angle Functions

In this section, we study a SCC of curves of fixed rotation index, localized curvature functions, and prescribed first-order boundary conditions. By localization, we mean that curvature functions will be restricted to some subspaces of \mathbb{L}^2 such as subspaces spanned by certain dominant harmonics. This space of curves will be used in the computation of a new type of elastica, which we refer to as *local elastica*. We carry out several experiments with localization in the frequency domain, but the discussion is more general.

4.1 V-Local Curves

All curves will have the same initial position $p_0 \in \mathbb{R}^2$ and initial value θ_0 of the angle function. Thus, it suffices to consider angle functions of the form $\theta(s) = \theta_0 + \varphi(s)$, where $\varphi: I \rightarrow \mathbb{R}$ satisfies $\varphi(0) = 0$. As before, the curve associated with $(\ell, \theta) \in \mathbb{R} \times \mathbb{H}^1$ is given by

$$(4.1) \quad \alpha(s) = p_0 + e^\ell \int_0^s e^{j\theta(t)} dt.$$

We wish to localize curvature functions and consequently angle functions, as well. What sub-

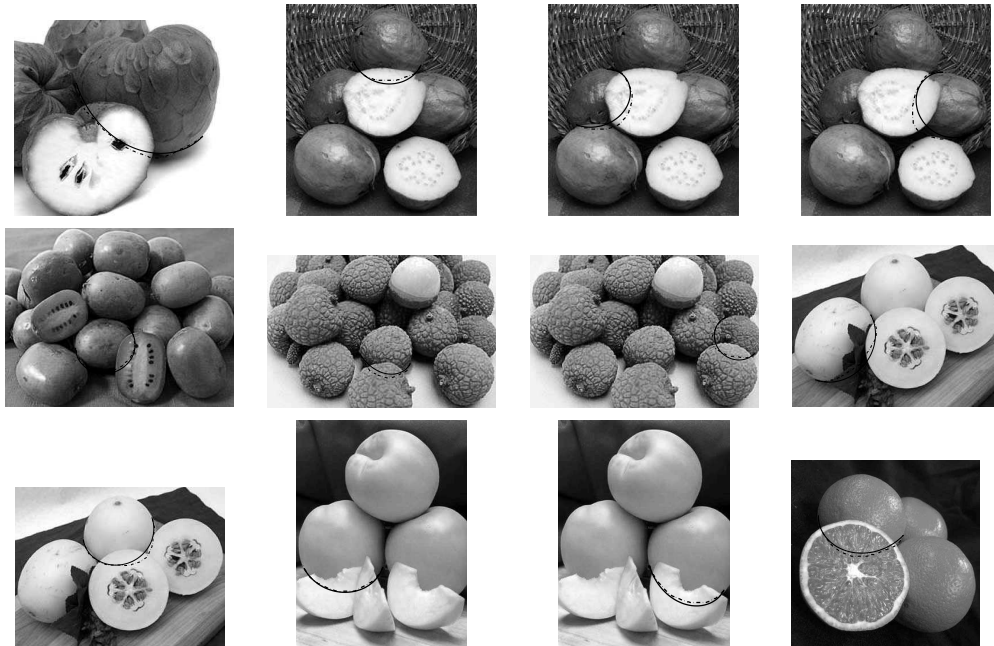


Figure 8: Examples of partial occlusions in natural images resolved with scale-invariant elasticae are shown as solid lines. Dashed lines are hand-drawn completions for comparison purposes.

spaces are we going to restrict angle functions to? This is equivalent to asking what restrictions the function φ should satisfy. We formulate the restrictions on φ in terms of the \mathbb{H}^1 inner product.

Since $\langle \varphi, 1 \rangle_1 = \varphi(0)$, functions $\varphi \in \mathbb{H}^1$ satisfying $\varphi(0) = 0$ are those orthogonal to constant functions. They can be written as $\varphi(s) = \int_0^s \varphi'(\xi) d\xi$. Hence, we localize angle functions as follows: pick a finite-dimensional subspace $W \subset \mathbb{L}^2$, with orthonormal basis $\{\sigma_1, \dots, \sigma_n\}$; this is to be interpreted as localizing $\kappa(s) = \theta'(s) = \varphi'(s)$ to W . If

$$(4.2) \quad \varphi_i(s) = \int_0^s \sigma_i(t) dt,$$

we restrict φ to the subspace $V = \text{span}\{\varphi_1, \dots, \varphi_n\}$ of \mathbb{H}^1 . In this paper, we only consider localization to finite-dimensional subspaces, but the construction can be extended to other subspaces.

Example. Let $W \subset \mathbb{L}^2$ be the subspace spanned by the truncated Fourier basis

$$\left\{ 1, \sqrt{2} \cos(2\pi s), \dots, \sqrt{2} \cos(2k\pi s), \sqrt{2} \sin(2\pi s), \dots, \sqrt{2} \sin(2k\pi s) \right\}.$$

If $\{\sigma_i\}_{i=1}^{2k+1}$ are these basis elements, use (4.2) to obtain a basis $\{\varphi_i\}_{i=1}^{2k+1}$ of V . This choice of W corresponds to localizing curvature functions to the first $2k+1$ harmonics. \square

We restrict our attention to V -local angle functions; that is, angle functions of the form

$$(4.3) \quad \theta(s) = \theta_0 + x_1 \varphi_1(s) + \dots + x_n \varphi_n(s),$$

where $x = (x_1, \dots, x_n) \in \mathbb{R}^n$. Thus, curves of length $L = e^\ell$, localized angle functions, and given first-order initial conditions can be represented by pairs $(\ell, x) \in \mathbb{R}^{n+1}$ via

$$(4.4) \quad \alpha(s) = p_0 + e^\ell \int_0^s e^{j(\theta_0 + \sum_{i=1}^n x_i \varphi_i(\tau))} d\tau.$$

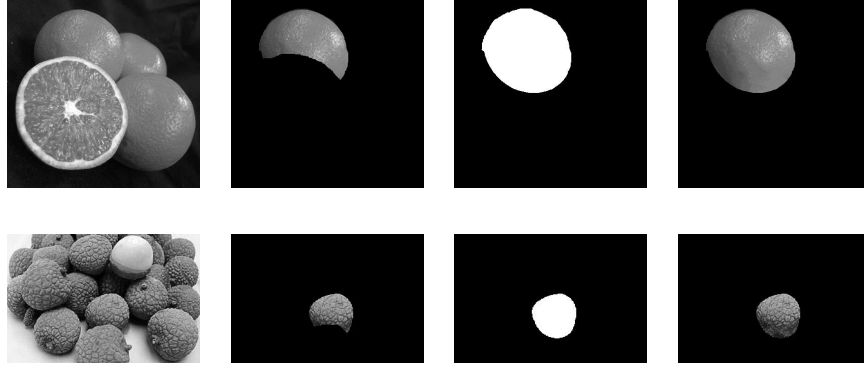


Figure 9: Each row shows an image of several fruits, the visible part of one of the partially occluded fruits, a completion of its contour with a scale-invariant elastica, and an analysis-synthesis extension of observed pixel values.

If $f_a = \sum_{i=1}^n x_i \varphi_i(s)$ and $f_b = \sum_{i=1}^n y_i \varphi_i(s)$, then $\langle f_a, f_b \rangle_1 = x_1 y_1 + \dots + x_n y_n$. Thus, the inner product $\langle (v, f_a), (w, f_b) \rangle$ defined in (2.5) can be expressed in terms of the pairs $(v, x), (w, y)$ as the standard Euclidean inner product

$$(4.5) \quad (v, x) \cdot (w, y) = vw + x_1 y_1 + \dots + x_n y_n$$

in \mathbb{R}^{n+1} .

As in Sec. 2, we are interested in curves with prescribed rotation index and first-order boundary conditions. Therefore, analogous to the constraints on pairs (ℓ, θ) imposed by the function F , defined in (2.6), we consider the map $G: \mathbb{R}^{n+1} \rightarrow \mathbb{R}^3$ given by:

$$(4.6) \quad G^1(\ell, x) = e^\ell \int_0^1 \cos \theta(s) ds; \quad G^2(\ell, x) = e^\ell \int_0^1 \sin \theta(s) ds; \quad G^3(\ell, x) = \theta(1),$$

with θ as in (4.3). Note that, in this representation, the value $\theta(0)$ is fixed to be θ_0 , so the condition on $\theta(0)$ is automatically satisfied. The relevant SCC of V -local curves is the iso-set $\mathcal{A}_V = G^{-1}(d_1, d_2, \theta_1)$, where $d = (d_1, d_2) \in \mathbb{R}^2$ is the desired total displacement $d = p_1 - p_0$. For almost all choices of V , \mathcal{A}_V is a smooth $(n-2)$ -dimensional submanifold of \mathbb{R}^{n+1} .

As in Sec. 2, a computation of the normal structure to level sets of the mapping G is needed for projections of points and vector fields in the ambient space \mathbb{R}^{n+1} onto \mathcal{A}_V . The mechanism is identical to that discussed earlier, so we just provide expressions for ∇G^i , $1 \leq i \leq 3$. Differentiating (4.6) and using (4.3), one obtains:

$$(4.7) \quad \begin{aligned} \nabla G^1(\ell, x) &= \left(G^1(\ell, x), -e^\ell \int_0^1 \varphi_1(s) \sin \theta(s) ds, \dots, -e^\ell \int_0^1 \varphi_n(s) \sin \theta(s) ds \right); \\ \nabla G^2(\ell, x) &= \left(G^2(\ell, x), e^\ell \int_0^1 \varphi_1(s) \cos \theta(s) ds, \dots, e^\ell \int_0^1 \varphi_n(s) \cos \theta(s) ds \right); \\ \nabla G^3(\ell, x) &= (0, \varphi_1(1), \dots, \varphi_n(1)). \end{aligned}$$

Algorithm 3 [Projection onto \mathcal{A}_V]: Given a curve representation $(\ell, x) \in \mathbb{R}^{n+1}$, we present an algorithm to project it onto \mathcal{A}_V , for a given d_1, d_2 , and θ_1 . Choose $\epsilon, \delta > 0$ small.

1. Compute $G(\ell, x)$ using Eqn. 4.6 and the residual vector $r(\ell, x) = (d_1, d_2, \theta_1) - G(\ell, x)$. If $\|r(\ell, x)\| < \epsilon$, then stop. Else, continue.
2. Compute $\nabla G^i(\ell, x) \in \mathbb{R}^{n+1}$, for $i = 1, 2, 3$, according to Eqn. 4.7.
3. Compute $(\dot{\ell}, \dot{x})$ according to: $(\dot{\ell}, \dot{x}) = \sum_{i=1}^3 r_i(\ell, x) \nabla G^i(\ell, x)$.
4. Update $(\ell, x) = (\ell, x) + \delta(\dot{\ell}, \dot{x})$. Return to Step 1.

4.2 V-Local Elasticae

If $(\ell, x) \in \mathbb{R}^{n+1}$ represents a V -local curve α with angle function $\theta(s) = \theta_0 + x_1\varphi_1(s) + \dots + x_n\varphi_n(s)$, then

$$\kappa(s) = \theta'(s) = x_1\sigma_1(s) + \dots + x_n\sigma_n(s).$$

Since $\{\sigma_i, 1 \leq i \leq n\} \subset \mathbb{L}^2$ is an orthonormal set, the scale-invariant elastic energy of α defined in (3.1) reduces to

$$(4.8) \quad E_{si}(\ell, x) = \frac{1}{2} (x_1^2 + \dots + x_n^2).$$

Thus, $\nabla_{\mathbb{R}^{n+1}} E_{si}(\ell, x) = (0, x_1, \dots, x_n)$. Subtracting normal components, we obtain the gradient field $\nabla_{\mathcal{A}_V} E_{si}$ on \mathcal{A}_V associated with the scale-invariant elastic energy. Flow lines of the negative gradient vector field approach V -local elasticae asymptotically.

Algorithm 4 [Finding Local Elastica]: Given boundary conditions in the form (d_1, d_2, θ_1) and a subspace V , find a local elastica satisfying the given boundary conditions. Initialize (ℓ, x) with a straight line between the end points.

1. Project (ℓ, x) onto \mathcal{A}_V using Algorithm 3.
2. Using Eqn. 4.7, compute $e_i \equiv \nabla G^i(\ell, x)$, for $i = 1, 2, 3$, and make them orthonormal in \mathbb{R}^{n+1} using Gram-Schmidt.
3. Compute the gradient vector $(0, x_1, \dots, x_n)$ and project it onto tangent space using:

$$(d\ell, dx) \equiv (0, x_1, \dots, x_n) - \sum_{i=1}^3 \langle (0, x_1, \dots, x_n), e_i \rangle e_i.$$

If $\|(d\ell, dx)\| < \epsilon$, stop. Else, continue.

4. For a step size $\delta > 0$, perform the update: $(\ell, x) = (\ell, x) + \delta(d\ell, dx)$. Return to Step 1.

Fig. 10 shows various scale-invariant elasticae computed with this algorithm. Each panel displays several elasticae with the same rotation index and first-order boundary conditions, but localized to different subspaces in the frequency domain. The subspace $W \subset \mathbb{L}^2$ is chosen to suppress all but a few fundamental harmonics in a Fourier representation of κ .

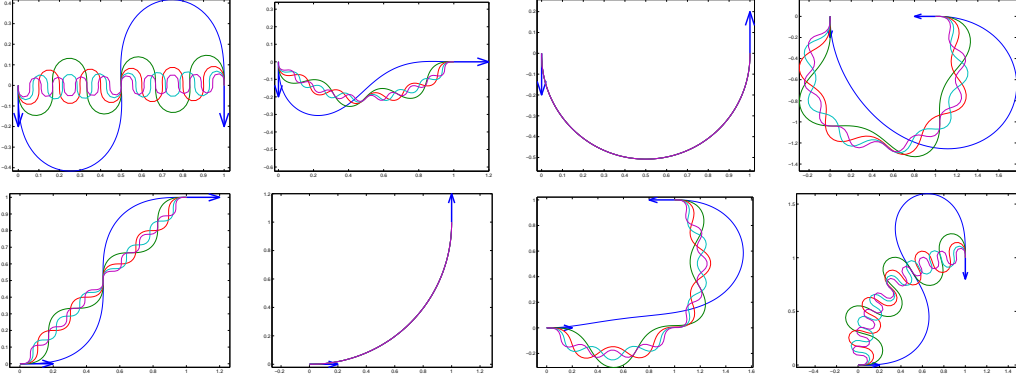


Figure 10: Each panel shows several examples of scale-invariant elasticae with the same boundary conditions and angle functions localized to different subspaces V .

5 Discovery of Contours and Appearances

As pointed out in Sec. 1, resolving partial occlusions of contours of objects in images with elasticae only yields good results in situations where hidden contours are small or not very rich in geometric features. This is because elasticae only take first-order boundary information into account and are designed to minimize the bending elastic energy. If additional contextual knowledge is unavailable, the problem of discovering shapes of hidden contours is very challenging. In such generality, it might be difficult to develop meaningful quantitative criteria to measure the “goodness” of a proposed completion.

We propose to use localization, in a Bayesian framework, to produce completions that take into consideration more information about the global geometry of visible contours. The basic idea is to restrict the search to curves whose curvature (or angle) functions contain just enough harmonics to capture the geometry of the visible portions, so that observed geometric patterns will propagate to the parts to be estimated without high energy costs. Several examples will illustrate the fact that, in the presence of periodic patterns, this technique leads to improved contour estimations. As in Sec. 3.2, estimations of contours will be combined with texture analysis and synthesis techniques to extend observed patterns of pixel values to the newly discovered regions.

5.1 A Manifold of Localized Closed Curves

To simplify the discussion, we assume that the visible portion of the contour of an imaged object has been extracted and consists of a single arc. Hence, we work under the hypothesis that the data is presented as a parametric curve γ . In addition, we suppose that the length of the part of the contour to be estimated is known, but the model can be modified to relax these assumptions.

Given an open curve $\gamma: [0, L_0] \rightarrow \mathbb{R}^2$, $L_0 > 0$, with unit-speed parameterization, we would like to find an optimal “completion” of γ to a closed curve α of rotation index 1 and length $L > L_0$. For the problem to be interesting, we assume that $L > \|\gamma(L_0) - \gamma(0)\| + L_0$. We let $\theta_\gamma: [0, L_0] \rightarrow \mathbb{R}$ be an angle function for the curve γ , $\theta_0 = \theta_\gamma(0)$, and $p_0 = \gamma(0)$.

In Sec. 4, V -local curves were represented by pairs $(\ell, x) \in \mathbb{R}^{n+1}$. Since we are assuming that the length L of the contour to be estimated is known, we can fix ℓ and work only with the variable

$x \in \mathbb{R}^n$. An n -tuple $x = (x_1, \dots, x_n)$ represents the constant-speed curve

$$\alpha(s) = p_0 + L \int_0^s e^{i\theta(t)} dt.$$

Here, $\theta: I \rightarrow \mathbb{R}$ is the angle function $\theta(s) = \theta_0 + \sum_{i=1}^n x_i \varphi_i(s)$, with φ_i as in (4.2). The curvature function of α is $\kappa(s) = (1/L) \sum_{i=1}^n x_i \sigma_i(s)$, where $\sigma_i(s) = \varphi_i'(s)$.

The SCC of interest can be thought of as a slice of the manifold \mathcal{A}_V of Sec. 1.3 consisting of all elements representing curves of the desired (fixed) length. The constraints that $x \in \mathbb{R}^n$ should satisfy are analogous to those in (4.6), but the expressions are simpler because ℓ is fixed. Let $H: \mathbb{R}^n \rightarrow \mathbb{R}^3$ be the map

$$(5.1) \quad H^1(x) = \int_0^1 \cos \theta(s) ds; \quad H^2(x) = \int_0^1 \sin \theta(s) ds; \quad H^3(x) = \theta(1) - \theta_0,$$

with $\theta(s) = \theta_0 + \sum_{i=1}^n x_i \varphi_i(s)$. The relevant SCC of V -local curves can be described as $\mathcal{H}_V = H^{-1}(0, 0, 2\pi)$. Elements of \mathcal{H}_V represent curves α with angle function θ satisfying: (i) $\alpha(0) = \gamma(0)$; (ii) $\theta(0) = \theta_0$; (iii) $\theta(1) = \theta_0 + 2\pi$. The gradient of H^i , $1 \leq i \leq 3$, is given by:

$$(5.2) \quad \begin{aligned} \nabla H^1(x) &= - \left(\int_0^1 \varphi_1(s) \sin \theta(s) ds, \dots, \int_0^1 \varphi_n(s) \sin \theta(s) ds \right); \\ \nabla H^2(x) &= \left(\int_0^1 \varphi_1(s) \cos \theta(s) ds, \dots, \int_0^1 \varphi_n(s) \cos \theta(s) ds \right); \\ \nabla H^3(x) &= (\varphi_1(1), \dots, \varphi_n(1)). \end{aligned}$$

As before, this calculation allows us to implement projections of points and vector fields in \mathbb{R}^n onto \mathcal{H}_V and solve optimization problems on \mathcal{H}_V using gradient methods.

Algorithm 5 [Projection onto \mathcal{H}_V]: Given a vector $x \in \mathbb{R}^n$, we present an algorithm to project it onto \mathcal{H}_V . Choose $\epsilon, \delta > 0$ small.

1. Compute $H(x)$ according to Eqn. 5.1 and the residual vector $r(x) = (0, 0, 2\pi) - H(x)$. If $\|r(x)\| < \epsilon$, then stop. Else, continue.
2. Compute $\nabla H^i(x)$, for $i = 1, \dots, 3$, according to Eqn. 5.2.
3. Compute \dot{x} according to: $\dot{x} = \sum_{i=1}^3 r_i(x) \nabla H^i(x)$.
4. Perform the update: $x = x + \delta \dot{x}$. Return to Step 1.

5.2 Bayesian Estimation of Contours

We take a Bayesian approach to the estimation of contours. We adopt a model having the scale-invariant elastic energy $E(x) = \frac{1}{2} \sum_{i=1}^n x_i^2$ as prior energy and data likelihood energy

$$F(\gamma|x) = \frac{1}{2} \int_0^{\zeta_0} (\theta(t) - \theta_\gamma(Lt))^2 dt,$$

where $\zeta_0 = L_0/L$. The functional $F(\gamma|x)$ quantifies the consistency of θ_γ with the angle function represented by $x \in \mathbb{R}^n$ over the interval $[0, L_0]$. For each λ , $0 < \lambda < 1$, the posterior energy is proportional to the functional

$$(5.3) \quad E_\lambda(x|\gamma) = \lambda F(\gamma|x) + (1 - \lambda)E(x).$$

We refer to a *maximum-a-posteriori* (MAP) estimation of the contour according to E_λ as a V -local λ -completion of γ . Equivalently, a λ -completion of γ is a curve represented by $x \in \mathcal{H}_V \subset \mathbb{R}^n$ that minimizes the posterior energy E_λ on the $(n-3)$ -dimensional manifold \mathcal{H}_V .

The estimation of V -local λ -completions requires that we solve an optimization problem on \mathcal{H}_V , which we approach with gradient methods. To simulate the negative gradient flow of E_λ on \mathcal{H}_V , we need to compute the partial derivatives of E_λ . For each $x \in \mathbb{R}^n$, let $W_x(s) = \theta(s) - \theta_\gamma(Ls)$, $0 \leq s \leq \zeta_0 = L_0/L$. Then,

$$(5.4) \quad \frac{\partial F}{\partial x_i} = \int_0^{\zeta_0} W_x(s) \varphi_i(s) ds \quad \text{and} \quad \frac{\partial E}{\partial x_i} = x_i.$$

Thus,

$$(5.5) \quad \nabla_{\mathbb{R}^n} E_\lambda(x) = \lambda \left(\frac{\partial F}{\partial x_1}, \dots, \frac{\partial F}{\partial x_n} \right) + (1 - \lambda) (x_1, \dots, x_n).$$

Projecting this vector orthogonally onto the tangent space $T_x \mathcal{H}_V$, we obtain $\nabla_{\mathcal{H}_V} E_\lambda(x)$. Flow lines of the negative gradient field on \mathcal{H}_V associated with E_λ approach λ -completions of γ asymptotically.

5.3 Algorithms and Experimental Results

Algorithm 6 [Finding V -Local Completions of Contours]: Given the visible curve γ and a basis $\{\varphi_i\}$ of V , find a local closed curve that minimizes the posterior energy. L_0 is the length of γ and L is the chosen length of its completion. Initialize $x \in \mathbb{R}^n$.

1. Project x onto \mathcal{H}_V using Algorithm 5.
2. Compute $e_i \equiv \nabla H^i(x)$, for $i = 1, 2, 3$, and make them orthonormal in \mathbb{R}^n using the Gram-Schmidt procedure.
3. Compute the gradient vector $\nabla_{\mathbb{R}^n} E_\lambda(x)$ using Eqn. 5.5 and project it onto the tangent space using:

$$dx \equiv \nabla_{\mathbb{R}^n} E_\lambda(x) - \sum_{i=1}^3 \langle \nabla_{\mathbb{R}^n} E_\lambda(x), e_i \rangle e_i.$$

If $\|dx\| < \epsilon$, stop. Else, continue.

4. For a step size $\delta > 0$, perform the update: $x = x + \delta dx$. Return to Step 1.

Fig. 11 shows a contour estimation obtained with this algorithm. The part of the contour of the starfish shown as a dotted line was hand extracted and represents the curve γ . To obtain a coarse estimation of the subspace V , we truncated the Fourier expansion of θ_γ keeping only the dominant harmonics and used the same fundamental harmonics to choose V . The first seven panels show the evolution of the curve during the gradient search and the last panel on the second row shows the MAP estimation of the contour. The first panel on the third row shows a plot of the angle function of γ and that of the estimated contour. The last panel displays the evolution of the posterior energy during the gradient search.

To illustrate the influence of the length on the MAP estimation, we carried out several other experiments with the same data. Fig. 12 shows several different V -local MAP contours obtained

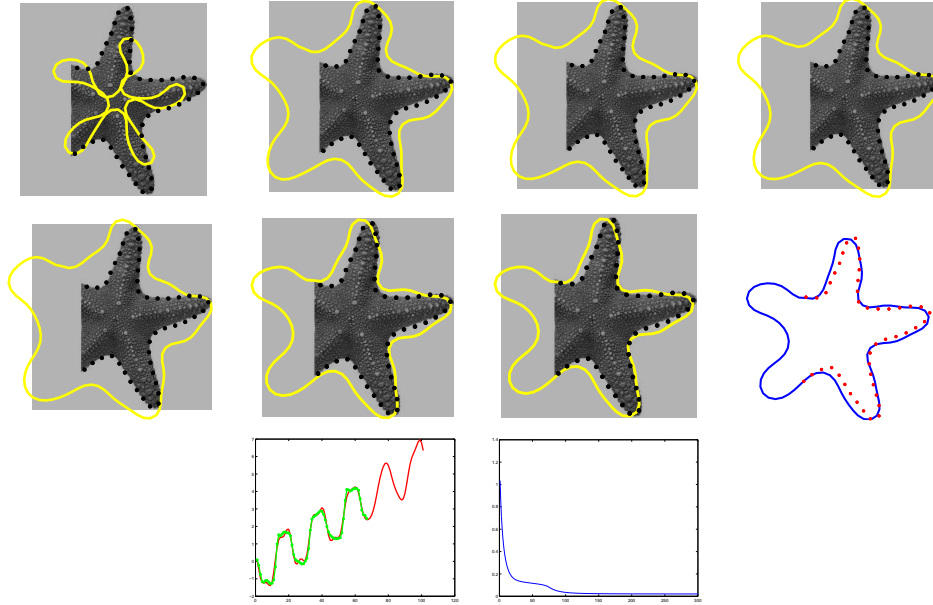


Figure 11: Various stages of a MAP estimation of the contour of a starfish. The hand-extracted data is shown as a dotted line. The first panel on the 3rd row shows a plot of the angle functions of the initial arc and the estimated contour. The last panel shows the evolution of the posterior energy.

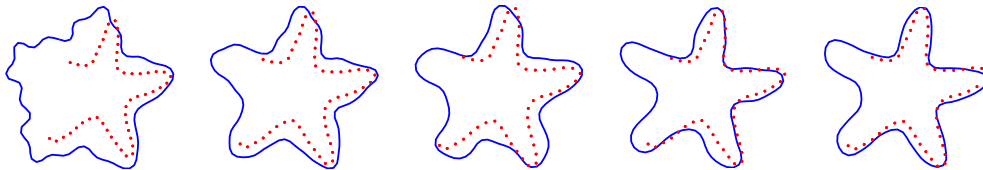


Figure 12: MAP estimations of various different lengths of the contour of a starfish. The length decreases from left to right.

with the same value of λ and subspace V , and decreasing values of L from left to right. The results indicate that the inference process is quite robust to variations of length. As pointed out above, the optimal choice of L can be automated by incorporating the length as a variable in the model.

The result of a similar Bayesian contour estimation experiment with an image of a flower is shown in Fig. 13. Results of experiments with estimations of full (shape-texture) appearances on three synthetic images are shown in Fig. 14.

6 Spaces of Localized Shapes

As discussed in Sec. 1.3, we wish to develop a framework for the multi-resolution analysis of closed, planar shapes using localization of angle functions. To simplify the discussion, we only consider localization in the frequency domain using truncated Fourier series, but the methods also apply to wavelet and other representations of functions.

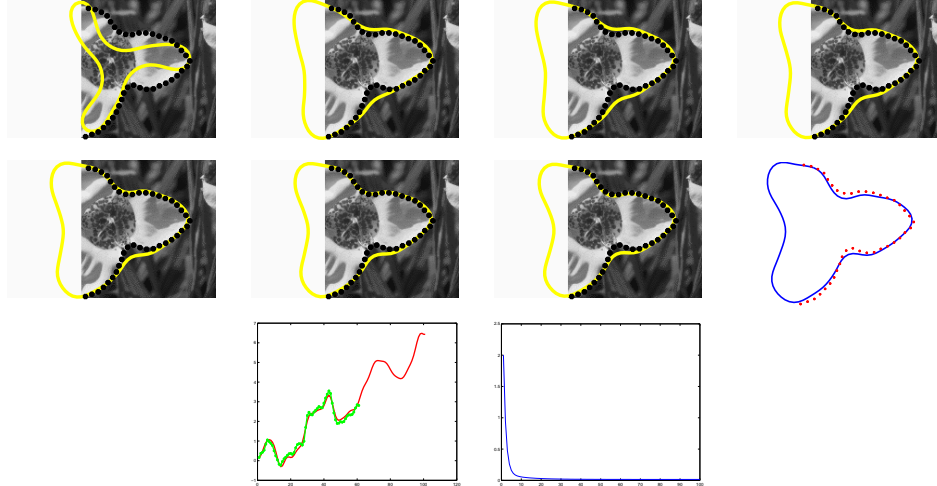


Figure 13: A MAP estimation of the contour of a flower.

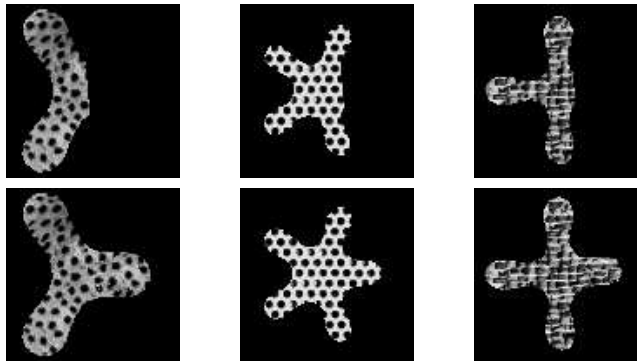


Figure 14: Joint contour-appearance estimations on synthetic data.

The shape of a planar contour is a property that is invariant under affine transformations of the plane; that is, compositions of translations, rotations and uniform scalings. (Reflections are treated separately, as explained below.) Thus, we seek representations of curves that are insensitive to these transformations. Given a parametric curve $\alpha: I \rightarrow \mathbb{R}^2$ with constant speed and length L , we represent α by an angle function $\theta: I \rightarrow \mathbb{R}$, which is characterized by $\alpha'(s) = Le^{j\theta(s)}$, for every $s \in I$. Angle functions are clearly invariant to translations and uniform scalings; the effect of a rotation is to add a constant to θ . As in [14], to remove variability due to rotations, we represent shapes using angle functions with fixed average, say, π . This corresponds to choosing a preferred rotational alignment of curves representing shapes.

We view the round circle as the simplest closed shape and adopt it as a basic reference. Thus, all spaces of localized angle functions will contain the angle function $\theta_c(s) = 2\pi s$ associated with the standard parameterization $\alpha(s) = (\cos(2\pi s), \sin(2\pi s))$ of the unit circle. For a given a positive integer n , we consider angle functions with average π whose deviations from θ_c are localized to the

first $2n$ Fourier components; they are of the form

$$(6.1) \quad \theta(s) = 2\pi s + \sum_{k=1}^n x_k \frac{\sin(2k\pi s)}{\sqrt{2}} + \sum_{k=1}^n y_k \frac{\cos(2k\pi s)}{\sqrt{2}},$$

where $x = (x_1, \dots, x_n), y = (y_1, \dots, y_n) \in \mathbb{R}^n$. (The constant term in this truncated Fourier representation is zero because both θ and θ_c have average π .) Thus, we represent θ with the pair $(x, y) \in \mathbb{R}^{2n}$. We are primarily interested in angle functions representing closed curves; that is, those satisfying $\int_0^1 e^{j\theta(s)} ds = 0$. Thus, analogous to the map H of Sec. 5.1, we let $J: \mathbb{R}^{2n} \rightarrow \mathbb{R}^2$ be given by

$$(6.2) \quad J^1(x, y) = \int_0^1 \cos \theta(s) ds \quad \text{and} \quad J^2(x, y) = \int_0^1 \sin \theta(s) ds,$$

with θ as in (4.3). Define the pre-shape space $\mathcal{P}_n \subset \mathbb{R}^{2n}$ as the level set $\mathcal{P}_n = J^{-1}(0, 0)$, which is an $(2n - 2)$ -dimensional submanifold of \mathbb{R}^{2n} consisting of pairs (x, y) associated with closed curves with localized angle functions.

As in [14], we refer to elements of \mathcal{P}_n as pre-shapes. This terminology is adopted because a shape may have multiple representatives in \mathcal{P}_n due to the variability in the choice of the initial point of the curve. Notice that once the initial point is fixed, so is the parameterization of the curve since we are assuming that α has constant speed. For each closed curve, there is a circle worth of possible initial points or parameterizations. Hence, changes of initial point may be viewed as an action of the unit circle \mathbb{S}^1 on \mathcal{P}_n . The shape space \mathcal{S}_n is the quotient space $\mathcal{P}_n/\mathbb{S}^1$ by the re-parameterization group \mathbb{S}^1 .

Again, we need two projection mechanisms for the manifold \mathcal{P}_n : projections of vectors $(v, w) \in \mathbb{R}^{2n}$ onto the tangent space $T_{(x,y)}\mathcal{P}_n$ and projections of points $(x, y) \in \mathbb{R}^{2n}$ onto \mathcal{P}_n . As before, these can be derived from a calculation of the gradient vectors

$$(6.3) \quad \nabla J^i = \left(\frac{\partial J^i}{\partial x_1}, \dots, \frac{\partial J^i}{\partial x_k}, \frac{\partial J^i}{\partial y_1}, \dots, \frac{\partial J^i}{\partial y_k} \right), \quad i = 1, 2.$$

Therefore, we compute the partial derivatives of J^i explicitly:

$$(6.4) \quad \begin{aligned} \frac{\partial J^1}{\partial x_k} &= -\frac{1}{\sqrt{2}} \int_0^1 \sin \theta(s) \sin(2k\pi s) ds; & \frac{\partial J^1}{\partial y_k} &= -\frac{1}{\sqrt{2}} \int_0^1 \sin \theta(s) \cos(2k\pi s) ds; \\ \frac{\partial J^2}{\partial x_k} &= \frac{1}{\sqrt{2}} \int_0^1 \cos \theta(s) \sin(2k\pi s) ds; & \frac{\partial J^2}{\partial y_k} &= \frac{1}{\sqrt{2}} \int_0^1 \cos \theta(s) \cos(2k\pi s) ds. \end{aligned}$$

6.1 Localization of Pre-Shapes

Given an angle function $\theta \in \mathbb{L}^2$ with average π representing a closed curve α , let

$$(6.5) \quad \theta(s) - 2\pi s = \sum_{k=1}^{\infty} a_k \frac{\sin(2k\pi s)}{\sqrt{2}} + \sum_{k=1}^{\infty} b_k \frac{\cos(2k\pi s)}{\sqrt{2}},$$

be the Fourier expansion of the deviation of θ from $\theta_c(s) = 2\pi s$. Truncating this expansion, we obtain the angle function

$$(6.6) \quad \bar{\theta}_n(s) = 2\pi s + \sum_{k=1}^n a_k \frac{\sin(2k\pi s)}{\sqrt{2}} + \sum_{k=1}^n b_k \frac{\cos(2k\pi s)}{\sqrt{2}}.$$

The pair $(a, b) \in \mathbb{R}^{2n}$ associated with this truncated function (or equivalently, $\bar{\theta}_n$) might not represent a closed curve. To close the curve, we project (a, b) onto \mathcal{P}_n to obtain $(x_\theta^n, y_\theta^n) \in \mathcal{P}_n$, which represents a localized pre-shape via Eqn. 4.3. This construction yields a localization procedure, namely, $\theta \mapsto (x_\theta^n, y_\theta^n)$.

Frequency localization of shapes is illustrated in Fig. 2. Each row shows a shape extracted from a natural image and the corresponding localizations at $n = 5, 10, 15$ and 20 , respectively. As the resolution increases (from left to right), localized shapes get closer to the original contour. Similar examples are shown in Fig. 15.

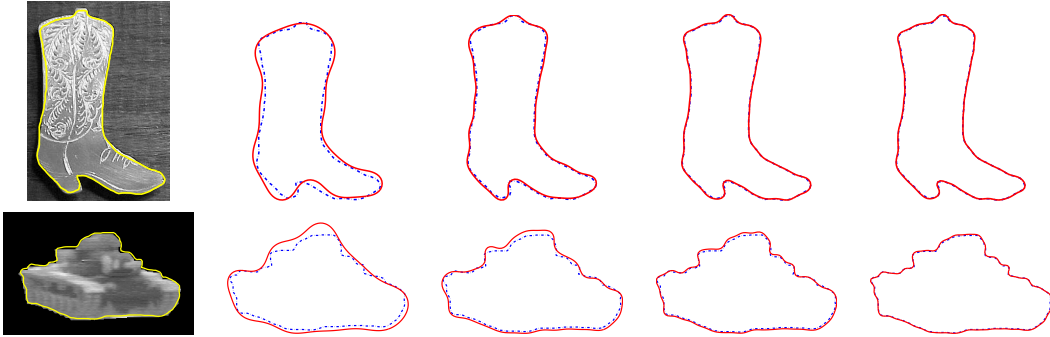


Figure 15: Shapes extracted from images are localized using $2n$ Fourier harmonics. The panels show localizations at $n = 5, 10, 15$ and 20 , with resolution increasing from left to right.

6.2 Geodesics in the Shape Space \mathcal{S}_n

We conclude our discussion of shapes with a description of an algorithmic procedure to calculate geodesics between any given pair of localized shapes. Once this is available, the methods of [14, 9, 20] can be readily adapted to yield techniques of multi-resolution, quantitative shape analysis. The approach to geodesics is similar to that adopted in the computation of geodesics in full (non-localized) shape space, but simpler and more efficient if the number of harmonics used is relatively small. Therefore, we just present the main ideas and refer the reader to [14] for further details.

Recall that shapes are elements of the quotient of the pre-shape space \mathcal{P}_n by the action of the group \mathbb{S}^1 of re-parameterizations. If $(x, y) \in \mathcal{P}_n$ and $z \in \mathbb{S}^1$, then the pre-shape obtained by the action of z on (x, y) is denoted $z \cdot (x, y)$. The \mathbb{S}^1 -orbit of (x, y) is the set

$$(6.7) \quad \mathcal{O}(x, y) = \{z \cdot (x, y) \mid z \in \mathbb{S}^1\} \subset \mathcal{P}_n.$$

Suppose that the pre-shapes $(x_0, y_0), (x_1, y_1) \in \mathcal{P}_n$ represent shapes $s_0, s_1 \in \mathcal{S}_n$, respectively. Then, any other pre-shape in the orbit of (x_i, y_i) , $i = 0, 1$, also represents s_i . The *geodesic distance*, $d(s_0, s_1)$, between s_0 and s_1 is defined as the infimum of the length of all paths in \mathcal{P}_n connecting a point in the orbit $\mathcal{O}(x_0, y_0)$ to a point in $\mathcal{O}(x_1, y_1)$.

It can be shown that the group \mathbb{S}^1 acts on \mathcal{P}_n by isometries; i.e., preserving distances in \mathcal{P}_n . This implies that the geodesic distance $d(s_0, s_1)$ can be computed as the infimum of the length of all paths in \mathcal{P}_n connecting (x_0, y_0) to a point in the orbit $\mathcal{O}(x_1, y_1)$; that is, it suffices to consider paths with fixed initial point (x_0, y_0) . Moreover, the distance $d(s_0, s_1)$ is realized by a geodesic in \mathcal{P}_n with initial point (x_0, y_0) , which is perpendicular to the \mathbb{S}^1 -orbit of (x_0, y_0) and whose terminal

point lies in $\mathcal{O}(x_1, y_1)$ – we refer to such geodesic as a geodesic in \mathcal{S}_n . Given these facts, we employ a *shooting method* to calculate geodesics in \mathcal{S}_n , as discussed next.

To describe the shooting method, we first introduce the *exponential map*. Let $(x, y) \in \mathcal{P}_n$ represent a pre-shape and $(v, w) \in T_{(x,y)}\mathcal{P}_n \subset \mathbb{R}^{2n}$ be a tangent vector to \mathcal{P}_n at (x, y) . Then, there is unique geodesic $\Psi(t; x, y, v, w)$ that starts at (x, y) and is tangent to (v, w) ; that is, $\Psi(0; x, y, v, w) = (x, y)$ and $\Psi'(0; x, y, v, w) = (v, w)$. The exponential map

$$\exp: T_{(x,y)}\mathcal{P}_n \rightarrow \mathcal{P}_n$$

is defined by $\exp(v, w) = \Psi(1; x, y, v, w)$. The map simply returns the position of the geodesic at time 1. With this terminology in place, the geodesic in \mathcal{S}_n from s_0 to s_1 can be constructed as follows:

- (i) Let $(x_0, y_0), (x_1, y_1) \in \mathcal{P}_n$ represent the shapes s_0 and s_1 , resp., and let O^\perp be the subspace of $T_{(x_0,y_0)}\mathcal{P}_n$ consisting of all vectors orthogonal to the orbit $\mathcal{O}(x_0, y_0)$ at (x_0, y_0) . Given a vector $(v, w) \in O^\perp$, calculate the geodesic $\Psi(t; x_0, y_0, v, w)$ by integrating the differential equation of geodesics in \mathcal{P}_n , numerically. If $\exp(v, w) \in \mathcal{O}(x_1, y_1)$ (i.e., the geodesic from (x_0, y_0) in the direction (v, w) reaches the orbit of (x_1, y_1) in unit time), then $\Psi(t; x_0, y_0, v, w)$, $0 \leq t \leq 1$ is the desired geodesic.
- (ii) Otherwise, consider the function $E: O^\perp \rightarrow \mathbb{R}$ given by

$$E(v, w) = \inf_{z \in \mathbb{S}^1} \|\exp(v, w) - z \cdot (x_1, y_1)\|^2.$$

The function E measures how far off the endpoint of the geodesic $\Psi(t; x_0, y_0, v, w)$, $0 \leq t \leq 1$, is from the desired target. The goal is to find the direction (v, w) that minimizes (or equivalently, annihilates) E . This minimization problem is solved using a gradient search on the subspace $O^\perp \subset T_{(x_0,y_0)}\mathcal{P}_n$.

Remark. To take the action of reflections into consideration in the calculation of geodesics between two shapes s_0 and s_1 , one can simply find the geodesic between s_0 and s_1 and the geodesic between s_0 and some reflection of s_1 and select the one with shortest length.

Fig. 16 shows geodesics morphing a flower into a duck at various different resolutions. The original shapes are shown in Fig. 2 and the deformations are given by geodesic paths in \mathcal{S}_n , for $n = 5, 10, 20$. The results of a similar experiment are shown in Fig. 17 for the boot and tank of Fig. 15. For the purpose of classifying and recognizing objects according to their shapes, an analysis at a lower resolution may prove to be sufficient.

7 Acknowledgments

This work was partially supported by the National Science Foundation and the Intelligence Technology Innovation Center through the grant DMS-0345242, and by the grants NSF (FRG) DMS-0101429 and NMA 201-01-2010.

References

- [1] Bruckstein, A.M. and Netravali, N.A.: On Minimal Energy Trajectories. *Computer Vision, Graphics and Image Processing* **49** (1990), 283–296.

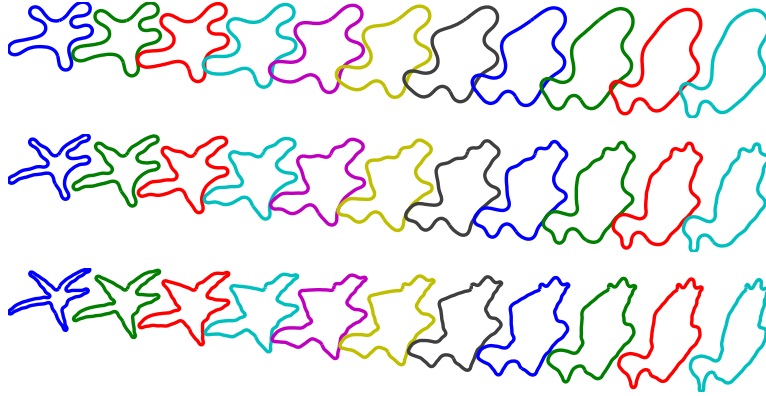


Figure 16: Geodesics between shapes computed at different resolutions. In the three rows, shapes are represented using 10, 20 and 40 harmonics, respectively. The original shapes are shown in Fig. 2.

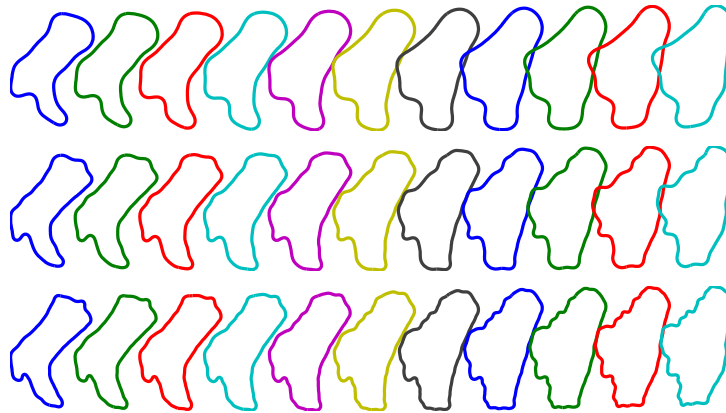


Figure 17: Geodesics between shapes computed at different resolutions. Shapes are represented using 10, 20 and 40 harmonics, respectively. The original shapes are shown in Fig. 15.

- [2] Chan, T., Shen, J., Vese, L.: Variational PDE Models in Image Processing. *Notices Amer. Math. Soc.* **50** (2003), 14–26.
- [3] Cremers, D., Soatto, S.: A Pseudo Distance for Shape Priors in Level Set Segmentation. In: *Proc. 2nd IEEE Workshop on Variational, Geometric, and Level-Set Methods in Computer Vision*, Nice, France (2003).
- [4] Cremers, D., Tischhäuser, F., Weickert, J., Schnörr, C.: Diffusion Snakes: Introducing Statistical Shape Knowledge into the Mumford-Shah Functional. *International Journal of Computer Vision* **50** (2002), 295–313.
- [5] Do Carmo, M.P.: *Differential Geometry of Curves and Surfaces*. Prentice Hall, Englewood Cliffs, NJ, 1976.
- [6] Dryden, I.L., Mardia, K.V.: *Statistical Shape Analysis*. John Wiley & Sons (1998).

- [7] Euler, L.: Methodus Inveniendi Lineas Curvas Maximi Minimive Proprietate Gaudentes, Sive Solutio Problematis Isoperimetrici Lattissimo Sensu Accepti. Bousquet, Lausannae e Genevae E65A. O. O. Ser. I, vol. 24 (1744).
- [8] Horn, B.P.K.: The Curve of Least Elastic Energy. ACM Trans. Math. Software **9** (1983), 441–460.
- [9] Joshi, S., Srivastava, A., Mio, W., Liu, X.: Hierarchical Organization of Shapes for Efficient Retrieval. In: Proc. 8th European Conference on Computer Vision. Prague, Czech Republic (2004).
- [10] Kanizsa, G.: Organization in Vision: Essays on Gestalt Perception. Praeger Scientific (1979).
- [11] Kass, M., Witkin, A., Terzopoulos, D.: Snakes: Active Contour Models. International Journal of Computer Vision **1** (1988), 321–33.
- [12] Kendall, D.G.: Shape Manifolds, Procrustean Metrics and Complex Projective Spaces. Bull. London Math. Society **16** (1984), 81–121.
- [13] Kimia, B.B., Frankel, I., Popescu, A.: Euler Spiral for Shape Completion. International Journal of Computer Vision **54** (2003), 159–182.
- [14] Klassen, E., Srivastava, A., Mio, W., Joshi, S.: Analysis of Planar Shapes Using Geodesic Paths on Shape Spaces. IEEE Trans. Pattern Analysis and Machine Intelligence **26** (2004), 372–383.
- [15] Langer, J., Singer, D.A.: Curve Straightening and a Minimax Argument for Closed Elastic Curves. Topology **24** (1985), 75–88.
- [16] Le, H.L., Kendall, D.G.: The Riemannian Structure of Euclidean Shape Spaces: a Novel Environment for Statistics. Annals of Statistics **21** (1993), 1225–1271.
- [17] Liu, X., Chen, R.: Independent Spectral Representations of Images for Recognition. J. Optical Soc. of America **20** (2003).
- [18] Maurel, P., Sapiro, G.: Dynamic Shapes Average. In: Proc. 2nd IEEE Workshop on Variational, Geometric, and Level-Set Methods in Computer Vision. Nice, France (2003).
- [19] Mio, W., Srivastava, A., Klassen, E.: Interpolations with Elasticae in Euclidean Spaces. Quarterly of Applied Mathematics, in press.
- [20] Mio, W., Srivastava, A., Liu, X.: Learning and Bayesian Shape Extraction for Object Recognition. In: Proc. 8th European Conference on Computer Vision. Prague, Czech Republic (2004).
- [21] D. Mumford, *Elastica and Computer Vision*, in Algebraic Geometry and its Applications (West Lafayette, IN, 1990), Springer, New York (1994), 491–506.
- [22] Palais, R.: Morse Theory on Hilbert Manifolds. Topology **2** (1963), 299–340.
- [23] Romeny, B.M., ed.: Geometry Driven Diffusion in Computer Vision. Kluwer Academic (1994).
- [24] Royden, H.L.: Real Analysis. Prentice Hall, 3rd edition (1988).
- [25] Sethian, J.: Level Set Methods: Evolving Interfaces in Geometry, Fluid Mechanics, Computer Vision, and Material Science. Cambridge University Press (1996).

- [26] Sharon, E., Brandt, A., Basri, R.: Completion Energies and Scale. *IEEE Trans. Pattern Analysis and Machine Intelligence* **15** (2000), 1117–1131.
- [27] Small, C.G.: *The Statistical Theory of Shape*. Springer-Verlag (1996).
- [28] Srivastava, A., Liu, X., Grenander, U.: Universal Analytic Forms for Modeling Image Probability. *IEEE Trans. on Pattern Analysis and Machine Intelligence* **28** (2002), 1200–1214.
- [29] Weiss, I.: 3D Shape Representation by Contours, *Computer Vision, Graphics and Image Processing* **41** (1988), 80–100.
- [30] Williams, L.R., Jacobs, D.W.: Stochastic Completion Fields: A Neural Model of Illusory Contour Shape and Saliency. In: *Proc. of the 5th Int. Conference on Computer Vision*, Boston, MA (1995) 408–415.
- [31] Williams, L.R., Jacobs, D.W.: Local Parallel Computation of Stochastic Completion Fields. *Neural Computation* **9** (1997), 837–858.
- [32] Wu, Y.N., Zhu, S.C., Liu, X.: Equivalence of Julesz Ensembles and FRAME models. *International Journal of Computer Vision* **38** (2000), 247–265.